



 Cite this: *RSC Adv.*, 2023, **13**, 28666

# A highly selective Hg<sup>2+</sup> colorimetric sensor and antimicrobial agent based on green synthesized silver nanoparticles using *Equisetum diffusum* extract

 Amina Jabbar,<sup>a</sup> Azhar Abbas,<sup>\*ac</sup> Nasir Assad,<sup>a</sup> Muhammad Naeem-ul-Hassan,<sup>\*a</sup> Hassan A. Alhazmi,<sup>de</sup> Asim Najmi,<sup>d</sup> Khalid Zoghebi,<sup>d</sup> Mohammed Al Bratty,<sup>d</sup> Ali Hanbashi<sup>f</sup> and Hatem M. A. Amin <sup>†\*b</sup>

Plasmonic nanoparticles such as Ag have gained great interest in the biomedical domain and chemical analysis due to their unique optical properties. Herein, we report a simple, cost-effective, and highly selective colorimetric sensor of mercury(II) based on *E. diffusum* (horsetail) extract-functionalized Ag nanoparticles (ED-AgNPs). The ED-AgNPs were synthesized by exploiting the coordination of Ag<sup>+</sup> with the various functional groups of ED extract under sunlight exposure for only tens of seconds. ED-AgNPs (63 nm) were characterized using various techniques such as UV-vis, FTIR, DLS, SEM and EDX. FTIR spectra suggested the successful encapsulation of the AgNPs surface with ED extract and XRD confirmed its crystalline nature. This ED-AgNPs colorimetric sensor revealed remarkable selectivity towards Hg<sup>2+</sup> in aqueous solution among other transition metal ions through a redox reaction mechanism. Besides, the sensor exhibited high sensitivity with rapid response and a detection limit of 70 nM. The sensor demonstrated feasibility for Hg(II) detection in spiked tap and river water samples. In addition, the synthesized ED-AgNPs revealed enhanced antimicrobial activity with higher efficacy against the Gram-positive bacterium (*L. monocytogenes* with an inhibition zone of 18 mm) than the Gram-negative bacterium (*E. coli* with an inhibition zone of 10 mm). The simplicity and adaptability of this colorimetric sensor render it a promising candidate for on-site and point-of-care detection of heavy metal ions in diverse conditions.

 Received 26th July 2023  
 Accepted 24th September 2023

DOI: 10.1039/d3ra05070j

[rsc.li/rsc-advances](http://rsc.li/rsc-advances)

## Introduction

Heavy metals, such as mercury, lead, cadmium, and arsenic are persistent pollutants that pose a significant danger to ecosystems and human health.<sup>1</sup> Hence, the development of reliable and sensitive methods for the monitoring and remediation of heavy metals is of utmost importance.<sup>2,3</sup> Conventional analytical methods for heavy metal detection such as ICP-MS often

require complex instrumentation, time-consuming sample preparation and high costs.<sup>4</sup> Therefore, there is a growing demand for simple, rapid and cost-effective detection methods to monitor heavy metal contaminations in various matrices.<sup>5,6</sup> Among others, colorimetric sensors have attracted considerable attention due to their simplicity, low cost, and ability to provide fast and visible readings for heavy metals detection.<sup>7-9</sup> In this regard, plasmonic metal nanomaterials such as silver nanoparticles (AgNPs) have attracted immense attention due to their distinct optical properties stemming from their localized surface plasmon resonance (LSPR), which is responsible for their characteristic color, rendering them promising candidates for the fabrication of colorimetric sensors.<sup>10-12</sup> However, many sensing nanoprobe are based on sophisticated synthesis routes of AgNPs, toxic chemicals, or complex composite materials, which would affect the reproducibility and stability of the analytical results.

The use of plant extracts for the synthesis of AgNPs has emerged as a green and sustainable alternative approach. This green approach avoids the use of hazardous chemicals and instead exploits the reducing and stabilizing capabilities of

<sup>a</sup>Institute of Chemistry, University of Sargodha, Sargodha 40100, Pakistan. E-mail: azhar.ramzan@uos.edu.pk; nakhan\_98@yahoo.com

<sup>b</sup>Chemistry Department, Faculty of Science, Cairo University, Giza 12613, Egypt

<sup>c</sup>Department of Chemistry, Government Ambala Muslim College, Sargodha 40100, Pakistan

<sup>d</sup>Department of Pharmaceutical Chemistry, College of Pharmacy, Jazan University, Jazan 82912, Saudi Arabia

<sup>e</sup>Substance Abuse and Toxicology Research Centre, Jazan University, Jazan 82912, Saudi Arabia

<sup>f</sup>Department of Pharmacology and Toxicology, College of Pharmacy, Jazan University, Jazan 82912, Saudi Arabia

<sup>†</sup> Present address: Faculty of Chemistry and Biochemistry, Ruhr University Bochum, Bochum 44801, Germany, E-mail: hatem.amin@rub.de


bioactive compounds present in plants, that are normally discarded in the trash.<sup>13–15</sup> Various plant extracts with different compositions and phytochemical profiles, such as those from *Olea europaea* L.,<sup>13</sup> *Pistacia atlantica*,<sup>16</sup> *Citrullus lanatus*,<sup>17</sup> *Myrsine africana* leaf<sup>18</sup> and *Spilanthes acmella* leaf<sup>19</sup> have been reported for the synthesis of Ag NPs. The use of biosynthesized Ag NPs as sensing probes for heavy metal ions such as Hg<sup>2+</sup> and Cu<sup>2+</sup> has gained enormous interest in the last decade.<sup>17</sup> For example, *Citrullus lanatus*-based Ag NPs were synthesized and further functionalized with 3-mercaptopropyl-1,2-propanediol (MPD).<sup>17</sup> These particles were utilized for the detection of Hg<sup>2+</sup> in the  $\mu\text{M}$  level in aqueous solutions based on color changes accompanied by the chelating ability of MPD with Hg<sup>2+</sup>. Hyacinth plant leaves were utilized for the biosynthesis of AgNPs (10 nm), which showed excellent selectivity towards Hg<sup>2+</sup> among other monovalent, divalent and trivalent cations with measurable concentrations down to 10 nM.<sup>20</sup> Interestingly, AgNPs modified with different plant extracts revealed different selectivity toward metal ions, indicating the key role of the functional groups of the extract in controlling the selectivity and performance of the colorimetric sensor.<sup>21</sup> We note that the type of the capping agent and particle size also play a crucial role in the ecotoxicity and dissolution of AgNPs.<sup>22</sup> However, the fate and environmental safety of nanosilver are still largely unresolved. Nevertheless, considering eco-design strategies during nanomaterials synthesis and application would sustain safer nanotechnologies.<sup>23</sup>

*Equisetum diffusum* (also known as Himalayan horsetail) is a species of the *Equisetum* that is the only living genus in the Equisetaceae family of vascular plants.<sup>24</sup> It is widely spread along the Himalayan mountains from Shimla to Tibet, Sikkim, Assam Meghalaya and India, and it is also found in Bhutan, Nepal, Pakistan and Japan.<sup>24</sup> Various types of *Equisetums* are utilized for medicinal purposes.<sup>25</sup> For example, it is used for barren women and antibacterial and antioxidant agent. It is used in traditional medicine to treat low blood pressure and inflammation, as a diuretic and homeostatic, and for lead detoxification.<sup>26</sup> Hence, the green fabrication of AgNPs using *E. diffusum* extracts via a simple synthetic approach would help to reduce the expenditure of consumables and costs of colorimetric sensors.

Furthermore, silver nanoparticles have gained significant interest as antibacterial agents against a wide range of bacterial strains.<sup>27</sup> For instance, AgNPs synthesized using *Equisetum arvense* leaf extract demonstrated significant antibacterial activity for *Staphylococcus aureus* and *Escherichia coli*, with inhibition zones of 24 and 18 mm, respectively.<sup>28</sup> However, the applied synthetic route was time-consuming (24 h).

Herein, we report a facile and environmentally friendly biosynthesis method of AgNPs using a polar extract of *E. diffusum* (ED) leaves as reducing and stabilizing agents and with the help of sunlight exposure for a very short time (30 s). The synthesized AgNPs were *in situ* functionalized with phytochemicals from the ED extract in one step. The successful synthesis of AgNPs capped with ED was evidenced using various techniques including UV-vis, FTIR, SEM, and EDX. Further, the sensing performance of the developed AgNPs-based sensor was

evaluated for the detection of various metal ions such as Cd, Pb and, Co ions. The results revealed excellent selectivity toward only Hg ions among other ions. The obvious change in the color of ED-AgNPs with the addition of only Hg ions enabled naked-eye monitoring of Hg ions. We also delve into the mechanism underlying the selective colorimetric response of ED-AgNPs toward Hg ions. Further, the suitability of the sensor for real water samples was demonstrated. Additionally, the antibacterial potential of these ED-AgNPs against a Gram-positive bacterium (*Listeria monocytogenes*) and a Gram-negative bacterium (*Escherichia coli*) was assessed. Thus, the unique optical properties of ED-AgNPs, combined with the reducing and stabilizing capabilities of plant extracts, enable the development of a simple and cost-effective sensing platform for potential applications in the industrial and health sectors.

## Experimental

### Preparation of *E. diffusum* leaves extract

The current research used *Equisetum diffusum* leaves that were gathered in the month of August from the Tehsil Mirali district, Khyber Pakhtunkhwa, Pakistan. Taxonomists from the Botany Department of the University of Sargodha confirmed the specimens' identities. The leaves were thoroughly washed with deionized water and then shade dried for ten days at 25 °C before grinding to powder and then passing through a fine sieve (US standard mesh number 70). The powder (5.0 g) was dissolved in deionized water (100 mL) for 5 h at room temperature in a volumetric flask. Afterward, the lipophilic compounds were eliminated from the filtered extract using *n*-hexane solvent. The aqueous extract was dried at 45 °C in an air-drying oven for further use. All extractions and solution preparations in this study were made using deionized water.

### Synthesis of *E. diffusum*-mediated silver nanoparticles (ED-AgNPs)

A polar extract of *E. diffusum* (22.2 mg) was added to 50 mL of deionized water. Then, 10 mL of this extract suspension was added to 10 mL of 1.0 mM AgNO<sub>3</sub> solution (99.98%, Merck, Germany). This mixture was then exposed to direct sunlight on clear sunny days outdoors for different time intervals and the reaction's development was frequently monitored. The color of the solution was turned from yellow to brownish throughout the growth of AgNPs. Afterward, the obtained solution was centrifuged at 10 000 rpm for 30 min. The solid precipitate of AgNPs at the bottom of the falcon tube was then washed with water and centrifuged again. This washing process was repeated five times to remove unreacted material. Some of these obtained pure solid AgNPs were used for characterization while the remaining part was sonicated after the addition of distilled water to obtain a suspension of pure AgNPs. This suspension was used as a stock solution of AgNPs for further experiments.

### Physico-chemical characterization of AgNPs

Fourier-transform infrared (FTIR) spectra of the ED abstract alone and the ED-capped AgNPs were recorded using the



Shimadzu FTIR-8400S spectrometer and KBr pellets method. To improve the signal-to-noise ratio, each spectrum reflects an average of 20 scans at a resolution of  $2\text{ cm}^{-1}$  in the range of  $4000\text{--}500\text{ cm}^{-1}$ . The morphology, particle size, elemental composition of ED-AgNPs were investigated using a scanning electron microscope SEM (JEOL JSM-5910) equipped with an energy-dispersive X-ray (EDX) unit. The SEM images were taken at an acceleration voltage of 15 kV. For the ED extract alone, the sample was coated with a thin gold layer to avoid charging the sample during SEM/EDX analysis. ImageJ software was used to measure the particle size from SEM images. For SEM measurements, the sample was drop cast on a clean glassy carbon plate and was then dried before imaging. Dynamic light scattering (DLS) and zeta potential measurements were carried out using a Zetasizer Nano ZS (Malvern Panalytical).

### Colorimetric sensing of heavy metal ions using ED-AgNPs

Different metal ion ( $\text{Pb}^{2+}$ ,  $\text{Cu}^{2+}$ ,  $\text{Ni}^{2+}$ ,  $\text{Cd}^{2+}$ ,  $\text{Na}^+$ ,  $\text{Ca}^{2+}$ ,  $\text{Co}^{2+}$  and  $\text{Hg}^{2+}$ ) solutions were added to ED-AgNPs suspension to examine the potential of synthesized ED-AgNPs for the selective detection of heavy metal ions in an aqueous solution. Separate test tubes containing ED-AgNPs suspension (1 mL) and different metal ion solution (1 mL of 1 mM) were used for this experiment. Directly afterward, UV-vis spectrum of each solution containing ED-AgNPs and metal ions was recorded. Any noticeable alteration in the UV-vis spectra or colour of ED-AgNPs suspension following the addition of metal ions may serve as the basis for the selective detection of that metal ion. For  $\text{Hg}^{2+}$ , a considerable color shift was noticed. Additionally, a calibration curve was created by recording the spectra for various concentrations of  $\text{Hg}^{2+}$  (10–120  $\mu\text{M}$ ) to determine the minimal concentration of  $\text{Hg}^{2+}$  that can be measured using the ED-AgNPs.

To assess the application of ED-AgNPs nano-probe for the quantification of  $\text{Hg}^{2+}$  in real water samples, spiked river and tap water samples were tested. The river water sample was collected from Jhelum River near Sargodha, Pakistan, whilst tap water was collected from the Chemistry Laboratory, University of Sargodha. Different concentrations of  $\text{Hg}^{2+}$  (40, 70 and 100  $\mu\text{M}$ ) were added to river and tap water samples and the proposed colorimetric sensor was applied to measure the  $\text{Hg}^{2+}$  levels in these samples. Each experiment was carried out in triplicate ( $n = 3$ ).

### Antibacterial activity of ED-AgNPs

To investigate the antibacterial activity of the synthesized Ag particles, the well diffusion method was applied for two common bacterial strains, namely *E. coli* (ATCC19115) and *L. monocytogenes* (ATCC13932) which were provided by the Microbiology Laboratory of Government College University in Faisalabad, Pakistan. The following procedure was used to determine the antibacterial properties of AgNPs: in 120 mL water, 6.3 g of nutritional agar was dissolved. Next, the agar solution and the Petri plates were autoclaved for 15 min at  $121^\circ\text{C}$ . Each Petri dish was sterilized, then 40 mL of agar solution was placed into it and frozen for 20 min. Afterward, using the

stick/spread plate method, the chosen bacterial strains were individually distributed into each Petri dish. The well diffusion method was used here where five wells were carved on the agar film using a sterile cork borer after the sticking. 30  $\mu\text{L}$  aliquot of the following solutions were added separately to the wells and the wells were marked as follows: A: water (negative control), B:  $1\text{ }\mu\text{g mL}^{-1}$  erythromycin (positive control), C: ED-AgNPs ( $1\text{ mg mL}^{-1}$ ), D: ED plant extract, or E:  $1\text{ }\mu\text{g mL}^{-1}$   $\text{AgNO}_3$  solution. The agar Petri plates were then incubated at  $37^\circ\text{C}$  for 24 h to allow bacterial growth. The antibacterial activity of all samples was then determined by measuring the diameter of the inhibition zones around the wells. The entire antibacterial measurements were carried out in a clean, sterile laboratory with laminar flow cabinets. The experiments were performed three times, and data were analyzed by a Student's *t*-test, and a value of  $p < 0.05$  was considered significant.

Further, the minimum inhibitory concentration (MIC) of green synthesized ED-AgNPs was determined using the method described in the guideline of the Clinical and Laboratory Standards Institute (CLSI).<sup>29</sup> In this study, *L. monocytogenes* and *E. coli* were used as Gram-positive and Gram-negative model strains, respectively. Both strains were cultured in Mueller Hinton (MH) broth media and incubated in a shaking incubator at  $37^\circ\text{C}$  for 24 h with 200 rpm agitation. The bacterial inoculums were adjusted to the concentration of  $10^5\text{ CFU mL}^{-1}$ . The MIC test of the green-synthesized AgNPs was performed using the standard broth microdilution method. For the MIC test,  $1\text{ mg mL}^{-1}$  stock solution of the synthesized AgNPs was initially prepared and then from it, the following series of diluted concentrations ranging from (200–20  $\mu\text{g mL}^{-1}$ ) were examined to identify the MIC. In addition, negative control experiments were performed: the first negative control tube contained only nutrient broth while, the second negative control experiment tube contained nutrient broth and AgNPs ( $200\text{ }\mu\text{g mL}^{-1}$ ) and, the positive control was performed using a nutrient broth medium inoculated with only bacterial inoculums without AgNPs. Afterward, all tubes were incubated at  $37^\circ\text{C}$  for 24 h. After the incubation step, the MIC value was taken as the lowest concentration of AgNPs (antibacterial agent) that makes complete inhibition to bacterial growth.

## Results and discussion

### Biosynthesis of *E. diffusum*-mediated AgNPs

In this work, we employed a polar extract of *E. diffusum* as a green reducing and capping agent to produce AgNPs with the aid of direct sunlight in a very short time, as illustrated in Fig. 1. When 1 mM  $\text{AgNO}_3$  solution was mixed with the ED extract under diffused sunlight exposure, electrons could be transferred from the ED to  $\text{Ag}^+$ . As a result,  $\text{Ag}^+$  ions in the solution were reduced to metallic silver ( $\text{Ag}^0$ ), and thus mainly the hydroxy and carboxylate groups in the extract bound to the Ag nuclei forming stable ED-capped AgNPs, as shown in Fig. 1. This procedure can thus be used as an alternative to the classical chemical and physical methods, thus avoiding the use of hazardous reducing agents or high temperatures which are harmful to the environment. By observing the color change of



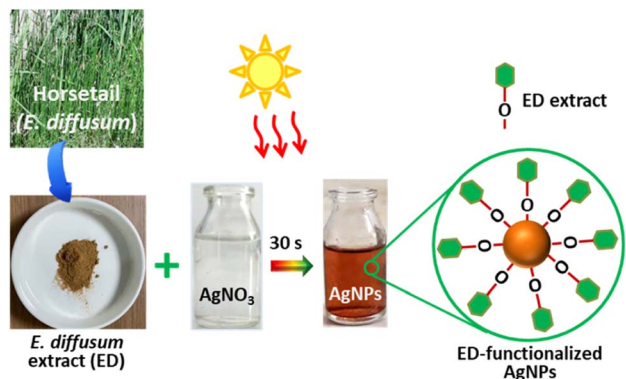


Fig. 1 Illustration of the green synthesis of ED-functionalized AgNPs using sunlight-mediated route.

the reaction mixture over time, we were able to track the growth of ED-AgNPs using the naked eye. In less than 60 s of sunlight exposure, the color of the solution containing ED extract and  $\text{AgNO}_3$  mixture went from colorless to reddish brown, and then dark brown, indicating the formation of AgNPs and inferring the reduction of all  $\text{Ag}^+$  ions, as displayed in Fig. 2a–c. We point out that when the reaction was carried out in the dark or at room temperature, no obvious reduction took place, indicating the essential role of sunlight irradiation in the completion of this reductive synthesis process.

Further, UV-vis spectrophotometry was used to evaluate the efficiency of *E. diffusum* extract in the mediated synthesis of ED-AgNPs, and consequently monitor the particles' growth. As depicted in Fig. 2d, the UV-vis spectra revealed a single characteristic peak centered at around 420 nm, which corresponds to the localized surface plasmon resonance (LSPR) of AgNPs. With the progress of time, absorbance maxima were recorded at 413, 435, 443, and 450 nm after 10, 15, 30, 45 and 60 s of exposure, respectively. This red shift of the absorption peaks in concurrent with an increase in the absorption indicates the progressive nucleation and growth of ED-AgNPs forming relatively larger particles with time. The mechanism of the formation of AgNPs using plant extract includes reduction, nucleation and growth steps, as described in detail in our previous work.<sup>13</sup> These results agree with our previous work on sunlight-mediated synthesis of AgNPs.<sup>12,13</sup> Hence, only a few tens of seconds of sunlight irradiations were needed to synthesize

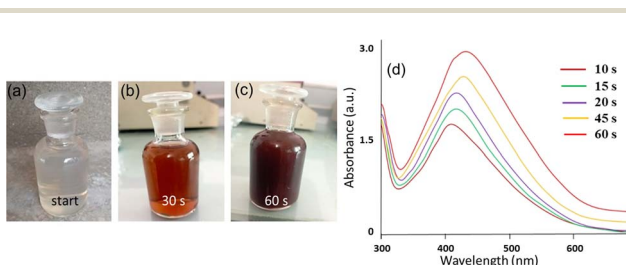


Fig. 2 Photographs of 1 mM  $\text{AgNO}_3$  + ED extract mixture after exposure to sunlight for (a) 0 s (start), (b) 30 s, and (c) 60 s showing color changes with time. (d) UV-vis spectra of ED-AgNPs suspension after different reaction times.

AgNPs *via* a simple, sustainable and cost-effective synthetic route, rendering our approach favourable over other classical chemical reduction or vapor deposition methods.

### Characterization of the synthesized ED-AgNPs

**FTIR and XRD analysis.** To analyze the functional groups and biomolecules present in the plant extract-modified nanoparticles and thus, confirm the involvement of phytochemicals in nanoparticle formation and stabilization, the FTIR spectrum of the bare ED extract was compared with that of the ED-AgNPs, as shown in Fig. 3a. We note that the synthesized sample was washed and centrifuged before analysis to isolate the AgNPs from free ED extract or other compounds present in the solution. The spectra of both samples are very similar with only slight shifts in the peak positions, as can be noticed from the peak wavenumbers. This similarity in peaks with the marginal peak shift proves the presence of the ED extract as a modifier of the AgNPs. For example, the C–H stretching band of alkanes at  $2920\text{ cm}^{-1}$  for the ED extract was shifted to  $2945\text{ cm}^{-1}$  for the ED-AgNPs. The hydroxyl groups (–OH) of phenols or carboxylic groups in the ED extract appeared as a broad band between  $3346$  and  $3510\text{ cm}^{-1}$ , whilst the –OH groups in the ED-AgNPs occurred at  $3518\text{ cm}^{-1}$ .<sup>30</sup> The peaks at  $1622$  or  $1614\text{ cm}^{-1}$  for both samples could be assigned to N–H amide bending, C=O stretching vibration or the stretching of aromatic rings.<sup>13,31</sup> The bands recorded at  $1085$  and  $1112\text{ cm}^{-1}$  for ED and ED-AgNPs, respectively, mostly correspond to C–N stretching of aliphatic amine.<sup>30</sup> The bands at  $1381$  and  $1413\text{ cm}^{-1}$  for the two materials could be assigned to C–N of an amine group or C–O of phenol.<sup>30</sup> The appearance of a peak at  $651\text{ cm}^{-1}$  might be related to O–Ag interaction in the ED-AgNPs. It is observed that some of the bands in the IR spectrum of ED-AgNPs were scaled down and slightly shifted as compared with the pure extract, which is an indication of the binding of  $\text{Ag}^+$  with the respective functional groups of the extract.<sup>32</sup> Thus, the bioactive compounds in the extract are possibly coordinated through hydroxyl and carbonyl groups or  $\pi$ -electrons to the metal.

Using GC-MS analysis, it is reported that ED extracts contain tens of potent bioactive compounds, including mainly phenolics, flavonoids, saponin and tannin.<sup>33,34</sup> These phyto-compounds are recognized to bind effectively with metal ions

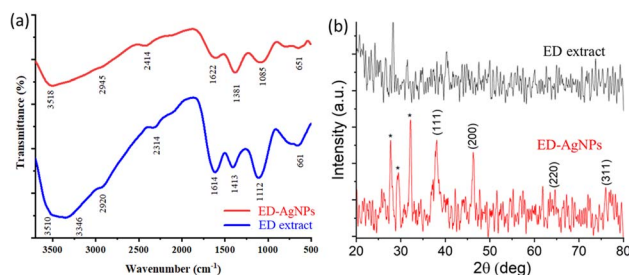


Fig. 3 (a) FTIR spectra and (b) XRD patterns of the bare ED extract and ED-AgNPs synthesized after 60 s exposure to diffused sunlight; asterisks mostly represent phases from the extract or a few  $\text{AgCl}$  deposits.



through their multiple functional groups. Thus, they are efficient in stabilizing AgNPs and are also desired for the selective detection of specific metal ions in water samples, as will be discussed below.

Furthermore, XRD analysis was performed to investigate the crystalline structure, phase, and purity of the synthesized ED-AgNPs. Fig. 3b presents a comparison of the XRD patterns of the sole ED extract and ED-AgNPs. XRD reflections at  $2\theta$  of  $38.1^\circ$ ,  $46.3^\circ$ ,  $46.5^\circ$  and  $75.9^\circ$  corresponding to (111), (200), (220) and (311) crystal planes, respectively, were observed, which are the common characteristic reflections of the face-centered cubic (fcc) structure of AgNPs (JCPDS, Card No. 04-0783).<sup>13,35</sup> This pattern, therefore, confirms that the AgNPs formed *via* the reduction of  $\text{Ag}^+$  by ED extract have crystalline nature. A few additional sharp peaks, marked with asterisks in the XRD pattern, were observed. The Bragg angles at  $27.7^\circ$  and  $32.1^\circ$ , match well the (111) and (200) planes of chlorargyrite fcc phase (JCPDS Card No. 31-1238), respectively, mostly suggesting the nucleation and growth of a few AgCl deposits onto or next to the main AgNPs. The remaining reflections are mostly attributed to the ED extract surrounding the NPs as they also appeared in the spectrum of the bare extract. XRD was also used to determine the crystallite size of the prepared NPs using Scherrer's equation:

$$D = \frac{K\lambda}{\beta \cos \theta} \quad (1)$$

where,  $D$  represents the crystallite size of the nanoparticle,  $\lambda$  denotes the wavelength of X-ray ( $\lambda = 0.154 \text{ nm}$  for Cu  $K_{\alpha 2}$ ),  $\beta$  is the full width at half maximum intensity (FWHM), and  $\theta$  accounts for Bragg's angle. The crystallite size obtained by

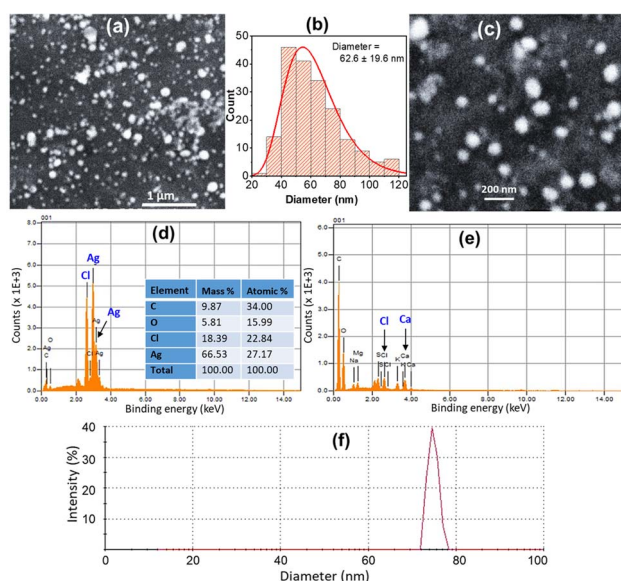


Fig. 4 (a and c) SEM images of ED-AgNPs with different magnifications. (b) Size distribution histogram with the longnorm curve; the average size  $\pm$  standard deviation is given. EDX spectrum of (d) ED-AgNPs and (e) ED extract; inset shows the elemental analysis from EDX. (f) DLS data of as-prepared ED-AgNPs.

analyzing various XRD peaks in the pattern was found to be 8–19 nm from different reflections.

**SEM-EDX characterization.** The morphology of the synthesized ED-AgNPs was examined using SEM, as shown in Fig. 4a and c. The recorded SEM images revealed the formation of spheroidal particles with no significant aggregation but with a few larger particles. To evaluate the particle size distribution, 193 particles from three independent micrographs (two are shown here) were analyzed and the corresponding histogram is displayed in Fig. 4b. An average particle size of  $62.6 \pm 19.6 \text{ nm}$  was obtained. This particle size agrees with the UV-vis data, where particles of tens of nanometers are expected for a plasmonic peak around 420 nm. Furthermore, the hydrodynamic particle size of the as-prepared ED-AgNPs was determined using DLS, as displayed in Fig. 4f, and a value of 76 nm was obtained. The hydrodynamic size is slightly larger than the size obtained from SEM analysis. This is expected and is attributed to the working principle of DLS measurement, where the solvation shell of the particles in solution is considered in the hydrodynamic size and DLS is an intensity-based measurement, whilst SEM gives a number distribution. Hence, DLS sizes should not involve a simple superposition with particle sizes from microscopy. Furthermore, a zeta potential of  $-31 \pm 3 \text{ mV}$  for the particles was obtained, indicating the colloidal stability of the pristine particles in water.

In addition, EDX spectra of the ED extract and the ED-AgNPs samples were recorded to identify the composition of the synthesized particles. EDX spectra (Fig. 4b) revealed the presence of strong signals of the Ag element in the ED-AgNPs sample, verifying the AgNPs formation. The EDX elemental analysis is given in the inset of Fig. 4b. In contrast, the Ag signal was absent for the bare plant extract. Notably, a strong Cl signal was detected in the EDX spectrum of AgNPs, while the ED spectrum did not exhibit such a strong Cl signal, likely suggesting the presence of minor chlorargyrite deposits. Besides, signals S, K, Ca, and Mg could be detected, which are most likely from phytochemical moieties in the extract. The intensity of C and O signals decreased for the capped AgNPs compared to the bare extract.

### Selective colorimetric detection of $\text{Hg}^{2+}$ using ED-AgNPs as a sensing assay

**Colorimetric detection of mercury(II) and analytical performance.** The ability of the synthesized ED-AgNPs to selectively detect heavy metal ions in an aqueous solution was achieved by utilizing the redox chemistry between  $\text{Hg}^{2+}$  and AgNPs. This interaction led to a significant change in the optical properties of the resulting AgNPs suspension, which was observable by the naked eye. Herein, we investigated the interaction of the synthesized ED-AgNPs with solutions containing various individual metal ions separately (namely, 1 mM of  $\text{Cd}^{2+}$ ,  $\text{Co}^{2+}$ ,  $\text{Pb}^{2+}$ ,  $\text{Ni}^{2+}$ ,  $\text{Cu}^{2+}$ , and  $\text{Hg}^{2+}$ ). Interestingly, the color of the suspension of AgNPs was unaffected with the addition of  $\text{Cd}^{2+}$ ,  $\text{Co}^{2+}$ ,  $\text{Ni}^{2+}$ ,  $\text{Cu}^{2+}$ , and  $\text{Pb}^{2+}$  solutions, see Fig. 5a. On the other hand, a striking rapid color change from reddish brown to colorless was observed by the naked eye only after the addition of  $\text{Hg}^{2+}$



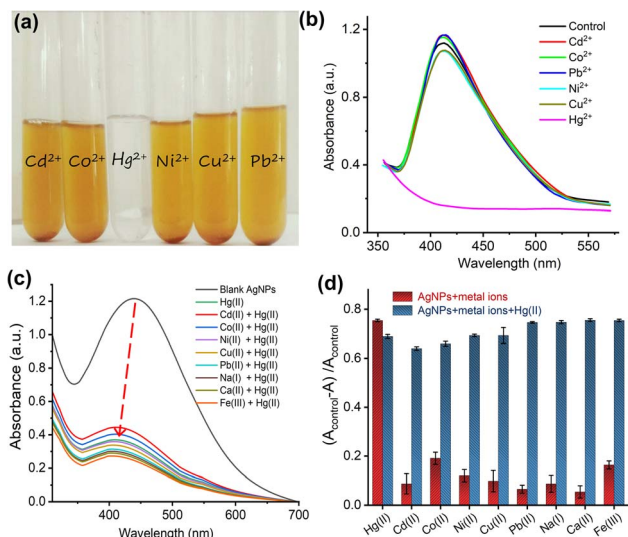


**Fig. 5** (a) Photographs of ED-AgNPs after the addition of 1 mM of  $\text{Cd}^{2+}$ ,  $\text{Co}^{2+}$ ,  $\text{Pb}^{2+}$ ,  $\text{Ni}^{2+}$ ,  $\text{Cu}^{2+}$ , and  $\text{Hg}^{2+}$  solutions. Control refers to ED-AgNPs suspension without metal ions. (b) Respective UV-vis spectra of the ED-AgNPs suspensions, showing the loss of color only with the addition of  $\text{Hg}^{2+}$ . (c) UV-vis spectra of AgNPs solution containing a binary mixture of  $80 \mu\text{M}$   $\text{Hg}^{2+}$  and 1 mM of other interfering metal ions. (d) Interference results in a bar chart diagram: red columns represent the absorbance change of AgNPs + metal ions from the blank, and the blue columns indicate the absorbance change of AgNPs + metal ions +  $\text{Hg}^{2+}$ . Error bars represent the standard deviation of three repeated measurements.

solution into the suspension of ED-AgNPs. The color change was further monitored using a UV-vis spectrophotometer. The UV-vis spectra of the corresponding solutions (Fig. 5b) clearly show the drastic decay and disappearance of the LSPR peak of AgNPs suspension at about 420 nm only upon the addition of  $\text{Hg}^{2+}$  solution, whereas the addition of  $\text{Cd}^{2+}$ ,  $\text{Co}^{2+}$ ,  $\text{Ni}^{2+}$ ,  $\text{Cu}^{2+}$ , and  $\text{Pb}^{2+}$  didn't show much change. Other ions such as  $\text{Ca}^{2+}$ ,  $\text{Na}^+$ , and  $\text{Fe}^{3+}$  were also tested and no interaction was observed. This demonstrates the high selectivity of the synthesized ED-capped AgNPs toward the detection of  $\text{Hg}^{2+}$ .

To further explore the influence of interfering metal ions on the selectivity of our sensing platform, an interference study was performed. Briefly, 1 mM of various metal ions (namely,  $\text{Cd}^{2+}$ ,  $\text{Co}^{2+}$ ,  $\text{Ni}^{2+}$ ,  $\text{Cu}^{2+}$ ,  $\text{Pb}^{2+}$ ,  $\text{Na}^+$ ,  $\text{Ca}^{2+}$ , and  $\text{Fe}^{3+}$ ) were added to the AgNPs suspension in the absence and presence of  $80 \mu\text{M}$   $\text{Hg}^{2+}$  and UV-vis spectra were recorded, as shown in Fig. 5c. The spectra show that in the presence of other metal ions, even with a higher concentration (13 molar equivalent), the interaction with  $\text{Hg}^{2+}$  didn't change, suggesting that other metal ions do not interfere with the detection of  $\text{Hg}^{2+}$ . Fig. 5d displays the change of absorbance of AgNPs + other metal ions solution from the blank in the absence (red bars) and presence (blue bars) of  $\text{Hg}^{2+}$ . The results revealed that only in the presence of  $\text{Hg}^{2+}$  in the AgNPs suspension an intensity change was observable and this change (*i.e.* interaction) wasn't influenced by interfering ions.

Furthermore, to create a calibration curve, the optical properties of ED-AgNPs suspension were studied after the

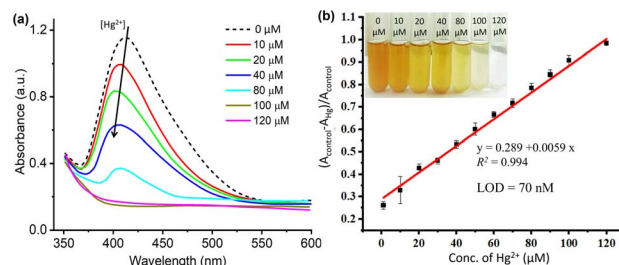


**Fig. 6** (a) UV-vis spectra of ED-AgNPs solution after the addition of different concentrations of mercury(II) ions. (b) Corresponding linear plot of the relative absorbance intensity difference at peak maxima versus  $\text{Hg}^{2+}$  concentration. Error bars represent the standard deviation of three repeated measurements. Inset: photograph of respective solutions at different concentrations.

addition of various concentrations of  $\text{Hg}^{2+}$  ions in the range from 10 to  $120 \mu\text{M}$ , as displayed in Fig. 6. By the naked eye, one can clearly observe a dilution of the brownish color as the concentration of  $\text{Hg}^{2+}$  in the solution increases, see inset of Fig. 6b. Besides, the UV-vis spectra were recorded for these different concentrations as shown in Fig. 6a. Notably, the intensity of the LSPR band around 420 nm of the AgNPs suspension decreased significantly as the concentration of  $\text{Hg}^{2+}$  increased. In addition, a blue shift of the LSPR band was observed upon the gradual increase of concentration. The observed blue shift is related to the Mie phenomenon, in which an increase in the Mie resonance frequency (*i.e.* a decrease of the LSPR wavelength) occurs with a decrease in the AgNPs size.<sup>36</sup> A similar effect was observed for AgNPs in previous works.<sup>37,38</sup> Even  $10 \mu\text{M}$   $\text{Hg}^{2+}$  (red line in Fig. 6a) showed obvious absorbance decay from the control measurement ( $0 \mu\text{M}$ , dashed black line).

The change in the LSPR band intensity from the control was quantitatively analyzed to establish a calibration curve. As shown in Fig. 6b, the absorbance difference increases linearly with increasing the concentration of  $\text{Hg}^{2+}$  in the studied range. From the slope of this linear regression, a limit of detection (LOD) of 70 nM was obtained. The LOD of our ED-AgNPs probe compares favorably to previously reported sensors. For example, higher LOD were reported for *Syzygium aqueum*-based AgNPs (LOD =  $0.85 \mu\text{M}$ ),<sup>37</sup> *p*-phenylenediamine-functionalized AgNPs (LOD =  $0.80 \mu\text{M}$ )<sup>39</sup> and *Agaricus bisporus*-capped AgNPs (LOD =  $2.1 \mu\text{M}$ )<sup>40</sup> and soap-root extract based AgNPs (LOD =  $2.2 \mu\text{M}$ ).<sup>38</sup> A comparable LOD (20–100 nM) was reported for 3-(Trimethoxysilyl) propyl methacrylate (TPPM) stabilized AgNPs.<sup>41</sup> Hence, this sensor not only compares favorably to many other sensing platforms but also is simple and highly selective.

### Analysis of $\text{Hg}^{2+}$ in real water samples using the proposed nano-probe

To explore the effectiveness of the sensor as an environmental monitoring system, real water samples were tested. The recovery of spiked  $\text{Hg}^{2+}$  in river water and tap water was established with the proposed ED-AgNPs sensor. Different concentrations ( $40$ ,  $70$ , and  $100 \mu\text{M}$ ) of  $\text{Hg}^{2+}$  were added to three



portions of both river and tap water samples. Afterward,  $\text{Hg}^{2+}$  recovery in these real water samples was examined using the same analytical procedure. The values of recovery and relative standard deviation (RSD) with a value of  $n = 3$  from actual water samples are summarized in Table 1. The obtained results confirm that the proposed ED-AgNPs nanoprobe could be an efficient and reliable sensor for the analysis of  $\text{Hg}^{2+}$  in real water samples.

**Proposed mechanism of Hg(n) sensing using AgNPs.** In principle, there are three main mechanisms for the detection of  $\text{Hg}^{2+}$  using AgNPs: (i) complexation and aggregation mechanism,<sup>39,41</sup> (ii) formation of Ag–Hg alloy<sup>42</sup> and (iii) redox reaction mechanism.<sup>5,37,38</sup> The latter is less discussed or considered in the literature. In the Ag–Hg alloy route,  $\text{Hg}(\text{n})$  reacts with Ag atoms of the AgNPs, forming Hg–Ag alloys. In the aggregation pathway, metal ions bind to the capping agent of the NPs, causing their aggregation and formation of larger particles. In the redox reaction process,  $\text{Hg}^{2+}$  reacts directly with  $\text{Ag}^0$  and oxidizes it to  $\text{Ag}^+$  (see Fig. 7). Both scenarios cause a decrease in the LSPR intensity, however, the redox reaction process led to a blue Mie shift of the band,<sup>38</sup> whilst the aggregation of AgNPs upon interaction with metal ions often causes a red shift and broadening of the LSPR band.<sup>41</sup> The capping agent of the NPs thus plays a role in directing the type of interaction of metal ions.

The suggested mechanism of  $\text{Hg}^{2+}$  sensing using our ED-AgNPs is mainly *via* the redox reactions between  $\text{Hg}^{2+}$  and Ag, as illustrated in Fig. 7, rather than the classical aggregation/coalescence mechanism. Our proposed mechanism is supported by the blue shift in the LSPR peak with increasing concentration, as displayed in Fig. 6a. Furthermore, after the addition of a small concentration (30  $\mu\text{M}$ ) of  $\text{Hg}^{2+}$  to AgNPs suspension, the particle size measured by DLS was decreased from 76 nm to 65 nm, inferring to size reduction (DLS doesn't necessarily give the absolute particle sizes but rather describes the trend). This mechanism is consistent with previous mechanisms underpinning the selective detection of  $\text{Hg}^{2+}$  using AgNPs.<sup>5,37,38</sup> Thus, the color change of the AgNPs solution could be attributed to the reduction of  $\text{Hg}^{2+}$  to  $\text{Hg}^0$  concurrent with the oxidation of the  $\text{Ag}^0$  in ED-AgNPs to  $\text{Ag}^+$ . Oxidation of Ag to  $\text{Ag}^+$  changes the color from reddish brown to colorless, as seen in the initial colorless  $\text{AgNO}_3$  solution (Fig. 1). The high selectivity of these ED-AgNPs to detect only mercury ions among others is explained by comparing the standard redox potentials

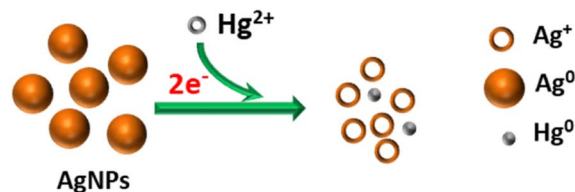
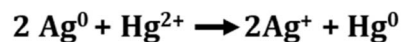


Fig. 7 Illustration of the proposed redox reaction mechanism underlying the colorimetric sensing of  $\text{Hg}^{2+}$  using ED-AgNPs.

of  $\text{Ag}^+/\text{Ag}$  (+0.80 V) and  $\text{Hg}^{2+}/\text{Hg}$  (+0.85) couples.<sup>43</sup> Since  $\text{Hg}^{2+}$  has a more positive reduction potential than  $\text{Ag}^+$ , it can oxidize Ag to  $\text{Ag}^+$ , whilst  $\text{Hg}^{2+}$  was reduced to metallic Hg particles, as presented in Fig. 7. Consequently, most transition metals and alkaline earth metals are unable to oxidize Ag atoms in the ED-AgNPs to  $\text{Ag}^+$  because of their more negative reduction potentials compared to Ag (+0.80 V), where  $\text{Pb}^{2+}$ ,  $\text{Co}^{2+}$ ,  $\text{Cd}^{2+}$ ,  $\text{Ni}^{2+}$  and  $\text{Cu}^{2+}$  have reduction potentials of  $-0.13$ ,  $-0.28$ ,  $-0.40$ ,  $-0.26$ ,  $-0.36$  V, respectively.<sup>43</sup> Thus, no color change was observed in the case of other metal ions. These results render this approach promising for the selective analysis of  $\text{Hg}^{2+}$ .

#### Evaluating the antibacterial activity of ED-AgNPs

Using the well diffusion method, the antibacterial properties of ED-AgNPs were studied against two harmful bacteria, namely *Listeria monocytogenes*, and *Escherichia coli*. AgNPs mediated by the polar extract of *E. diffusum* showed significant antibacterial

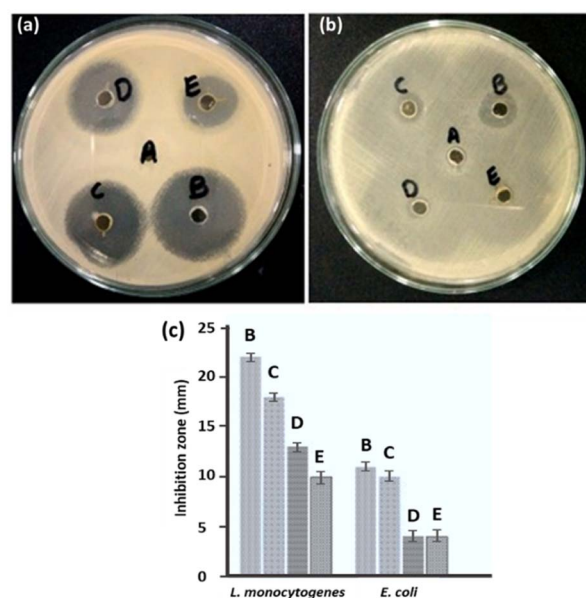


Fig. 8 Photographs showing the inhibition zones of (a) *L. monocytogenes* and (b) *E. coli* obtained for the (A) negative control, (B) positive control, (C) ED-AgNPs, (D) ED extract, and (E)  $\text{AgNO}_3$ . (c) Comparison of the measured inhibition zones for all the cases; error bars of repeated experiments are displayed.

Table 1 Analytical results for the detection of  $\text{Hg}^{2+}$  using ED-AgNPs based nano-probe in real water samples

Sample	$\text{Hg}^{2+}$ added ( $\mu\text{M}$ )	$\text{Hg}^{2+}$ found ( $\mu\text{M}$ )	Recovery (%)	RSD (%) $n = 3$
River water	40	38.4	96	5.3
	70	66.5	95	4.6
	100	95.3	95.3	6.6
Tap water	40	37.7	94.3	4.6
	70	64.2	91.7	6.3
	100	94.3	94.3	3.9



efficacy against *L. monocytogenes* and *E. coli*, as depicted in Fig. 8. The measured zone of inhibition (ZOI) for all cases is compared in a column diagram in Fig. 8c. For all studied cases, the inhibition efficacy against *L. monocytogenes* bacteria is double that of *E. coli*, as shown in the comparison in Fig. 8c. ED-AgNPs demonstrated larger ZOI for *L. monocytogenes* (18 mm) than *E. coli* (ZOI = 10 mm). It is obvious that larger inhibition zones indicate stronger antibacterial activity. It is important to run appropriate control experiments to ensure the reliability of the results. Therefore, the antibacterial properties of a negative control of the solvent water, a positive control of a standard antibacterial agent (erythromycin), bare AgNO<sub>3</sub> and bare ED extract were investigated, as shown in Fig. 8. The synthesized ED-capped AgNPs revealed significantly larger ZOI (18 and 10 mm) than only the ED extract (13 and 4 mm) or AgNO<sub>3</sub> (10 and 4 mm) and comparable inhibition zones to the standard antibacterial agent erythromycin (22 and 11 mm) against *L. monocytogenes* and *E. coli*, respectively.

Compared to relevant capped-AgNPs that were previously reported in the literature, our ED-AgNPs exhibited better or comparable antibacterial performance: for example, citrate-capped AgNPs showed ZOI of 7 mm for *E. coli*,<sup>44</sup> corn leaf extract-AgNPs had a ZOI of 11 mm against *E. coli* and 9 mm against *L. monocytogenes*,<sup>45</sup> sulfonamide-modified AgNPs revealed ZOI of 23 mm (ref. 12) and *V. officinalis*-modified AgNPs demonstrated ZOI of 9–15 mm against *L. monocytogenes*.<sup>46</sup>

Further, the MICs of AgNPs against *L. monocytogenes* and *E. coli* were evaluated in the present study using the broth dilution assay. The MIC values are given in Table 2. The obtained MICs of green synthesized AgNPs for *L. monocytogenes* and *E. coli* were 20 µg mL<sup>-1</sup> and 100 µg mL<sup>-1</sup>, respectively, showing that the synthesized AgNPs effectively inhibited the growth of these two pathogens at relatively low concentrations. The current MIC results show that Gram-negative bacterium (*E. coli*) is more resistant to AgNPs than Gram-positive bacterium (*L. monocytogenes*), in agreement with previous reports.<sup>47</sup> This might be attributed to variations in their cell wall composition or that the positive charges on AgNPs are trapped and blocked by lipopolysaccharides, thus making *E. coli* less susceptible to AgNPs. These data manifest the promising antibacterial activity of ED-AgNPs toward the studied bacteria. The enhanced antibacterial activity could be attributed to the larger exposed surface area of the nanoparticles and the inhibitive effectiveness of the bioactive compounds in the extract capping the NPs.

The most common antibacterial mechanism of AgNPs was described in our previous work.<sup>13</sup> Briefly, the mechanism involves the adsorption of the NPs onto the surface of the bacteria, followed by their entry into the bacterial cell due to

their small size. AgNPs can disrupt the bacterial membrane and create holes in it. Further, AgNPs can interact with intracellular proteins generating reactive oxygen species (ROS) that cause oxidative stress and cell damage.<sup>48</sup> They can also interact with proteins, enzymes, and DNA, disrupting their function. Similar interactions and cell damage could happen with the released Ag<sup>+</sup> ions from the AgNPs.

## Conclusions

A highly selective mercury colorimetric sensor based on green-synthesized AgNPs using ED extract, that is normally discarded in the trash, was developed. This study demonstrates the potential of utilizing plant extracts and sunlight irradiation in a simple, eco-friendly approach for the synthesis of stable functionalized-AgNPs, making it a viable alternative to the harmful conventional chemical synthesis routes. The synthesis *via* sunlight required only tens of seconds of exposure. The ED extract not only acts as a capping and reducing agent but also imparts unique surface properties to the AgNPs, promoting their selectivity and sensitivity to Hg<sup>2+</sup>. The successful synthesis of spheroidal crystalline ED-AgNPs particles was demonstrated by various characterization techniques such as FTIR, UV-vis, SEM, and XRD. Interestingly, this AgNPs probe generated by the polar extract of ED extract revealed remarkable selectivity toward only Hg<sup>2+</sup> ions. In addition, the developed sensor exhibited excellent sensitivity with rapid response and a detection limit at the nanomolar level for Hg<sup>2+</sup>. The interference study proved that the sensing of Hg<sup>2+</sup> was not affected by other cations. Importantly, the developed sensor successfully demonstrated suitability for Hg(II) quantification in real water samples. The *in situ* one-step functionalization of AgNPs with phytochemicals from the ED extract contributes to promoting their interaction and sensing ability. A non-common sensing mechanism based on the redox reaction between Ag and Hg was revisited and discussed. Furthermore, ED-AgNPs showed promising antibacterial activity when compared to AgNO<sub>3</sub> solution, plant extract solution, and the standard antibiotic agent erythromycin. Gram-positive bacteria demonstrated higher resistance to AgNPs than Gram-negative bacteria. Hence, the green-synthesized ED-AgNPs-based sensor holds great potential for various environmental applications.

## Author contributions

A. J.: investigation, writing—original draft; A. A.: methodology, supervision, resources, conceptualization, writing—review and editing; N. A.: investigation; M. N.-u.-H.: mentoring, formal analysis; H. A. A.: antibacterial data interpretation, resources, review and editing; A. N.: data interpretation, visualization; K. Z.: review and editing the Biosynthesis and Characterization section; M. A.: review and editing Characterization; A. H.: review and editing Antibacterial activity section; H. M. A. A.: conceptualization, mentoring, visualization, writing—review and editing. All authors have read and agreed to the published version of the manuscript.

**Table 2** Results of the inhibition zones and the MIC for both *L. monocytogenes* and *E. coli* obtained at ED-AgNPs

Bacteria	Zone of inhibition (mm)	MIC (µg mL <sup>-1</sup> )
<i>L. monocytogenes</i>	18	20
<i>E. coli</i>	11	100





## Conflicts of interest

There are no conflicts to declare.

## Acknowledgements

The authors extend their appreciation to the Deputyship for Research & Innovation, Ministry of Education in Saudi Arabia for funding this research work through the project number ISP23-90.

## References

- 1 C. T. Driscoll, R. P. Mason, H. M. Chan, D. J. Jacob and N. Pirrone, Mercury as a global pollutant: sources, pathways, and effects, *Environ. Sci. Technol.*, 2013, **47**, 4967–4983.
- 2 A. L. Suherman, E. E. Tanner and R. G. Compton, Recent developments in inorganic Hg<sup>2+</sup> detection by voltammetry, *TrAC, Trends Anal. Chem.*, 2017, **94**, 161–172.
- 3 A. L. Suherman, G. Zampardi, H. M. A. Amin, N. P. Young and R. G. Compton, Tannic acid capped gold nanoparticles: capping agent chemistry controls the redox activity, *Phys. Chem. Chem. Phys.*, 2019, **21**, 4444–4451.
- 4 A. Ono and H. Togashi, Highly selective oligonucleotide-based sensor for mercury(II) in aqueous solutions, *Angew. Chem., Int. Ed.*, 2004, **43**, 4300–4302.
- 5 A. L. Suherman, K. Ngamchuea, E. E. L. Tanner, S. V. Sokolov, J. Holter, N. P. Young and R. G. Compton, Electrochemical Detection of Ultratrace (Picomolar) Levels of Hg<sup>2+</sup> Using a Silver Nanoparticle-Modified Glassy Carbon Electrode, *Anal. Chem.*, 2017, **89**, 7166–7173.
- 6 B. M. May, M. F. Bambo, S. S. Hosseini, U. Sidwaba, E. N. Nxumalo and A. K. Mishra, A review on I-III-VI ternary quantum dots for fluorescence detection of heavy metals ions in water: optical properties, synthesis and application, *RSC Adv.*, 2022, **12**, 11216–11232.
- 7 N. A. Azmi, S. H. Ahmad and S. C. Low, Detection of mercury ions in water using a membrane-based colorimetric sensor, *RSC Adv.*, 2018, **8**, 251–261.
- 8 R. Paw, M. Hazarika, P. K. Boruah, A. J. Kalita, A. K. Guha, M. R. Das and C. Tamuly, Highly sensitive and selective colorimetric detection of dual metal ions (Hg<sup>2+</sup> and Sn<sup>2+</sup>) in water: an eco-friendly approach, *RSC Adv.*, 2021, **11**, 14700–14709.
- 9 X. Gong, Y. Bi, Y. Zhao, G. Liu and W. Y. Teoh, Graphene oxide-based electrochemical sensor: a platform for ultrasensitive detection of heavy metal ions, *RSC Adv.*, 2014, **4**, 24653–24657.
- 10 A. Abbas and H. M. Amin, Silver nanoparticles modified electrodes for electroanalysis: An updated review and a perspective, *Microchem. J.*, 2022, **175**, 107166.
- 11 K. Ngamchuea, C. Batchelor-McAuley, S. V. Sokolov and R. G. Compton, Dynamics of Silver Nanoparticles in Aqueous Solution in the Presence of Metal Ions, *Anal. Chem.*, 2017, **89**, 10208–10215.
- 12 S. Amin, M. Sher, A. Ali, M. F. Rehman, A. Hayat, M. Ikram, A. Abbas and H. M. Amin, Sulfonamide-functionalized silver nanoparticles as an analytical nanoprobe for selective Ni(II) sensing with synergistic antimicrobial activity, *Environ. Nanotechnol., Monit. Manage.*, 2022, **18**, 100735.
- 13 S. Ullah, R. Khalid, M. F. Rehman, M. I. Irfan, A. Abbas, A. Alhoshani, F. Anwar and H. M. A. Amin, Biosynthesis of phyto-functionalized silver nanoparticles using olive fruit extract and evaluation of their antibacterial and antioxidant properties, *Front. Chem.*, 2023, **11**, 1202252.
- 14 P. Banerjee, M. Satapathy, A. Mukhopadhyay and P. Das, Leaf extract mediated green synthesis of silver nanoparticles from widely available Indian plants: synthesis, characterization, antimicrobial property and toxicity analysis, *Bioresour. Bioprocess.*, 2014, **1**, 3.
- 15 S. Simon, N. R. S. Sibuyi, A. O. Fadaka, S. Meyer, J. Josephs, M. O. Onani, M. Meyer and A. M. Madiehe, Biomedical Applications of Plant Extract-Synthesized Silver Nanoparticles, *Biomedicines*, 2022, **10**, 2792.
- 16 B. Sadeghi, A. Rostami and S. S. Momeni, Facile green synthesis of silver nanoparticles using seed aqueous extract of *Pistacia atlantica* and its antibacterial activity, *Spectrochim. Acta, Part A*, 2015, **134**, 326–332.
- 17 S. Maiti, G. Barman and J. Konar Laha, Detection of heavy metals (Cu<sup>2+</sup>, Hg<sup>2+</sup>) by biosynthesized silver nanoparticles, *Appl. Nanosci.*, 2016, **6**, 529–538.
- 18 Q. Sarwer, M. S. Amjad, A. Mehmood, Z. Binish, G. Mustafa, A. Farooq, M. F. Qaseem, F. Abasi and J. M. La Pérez de Lastra, Green Synthesis and Characterization of Silver Nanoparticles Using *Myrsine africana* Leaf Extract for Their Antibacterial, Antioxidant and Phytotoxic Activities, *Molecules*, 2022, **27**, 7612.
- 19 F. Lalsangpuii, S. L. Rokhum, F. Nghakliana, L. Fakawmi, J. V. L. Ruatpuia, E. Laltnanmawii, R. Lalfakzuala and Z. Siana, Green Synthesis of Silver Nanoparticles Using *Spilanthes acmella* Leaf Extract and its Antioxidant-Mediated Ameliorative Activity against Doxorubicin-Induced Toxicity in Dalton's Lymphoma Ascites (DLA)-Bearing Mice, *ACS Omega*, 2022, **7**, 44346–44359.
- 20 O. S. Oluwafemi, J. L. Anyik, N. E. Zikalala and E. H. M. Sakho, Biosynthesis of silver nanoparticles from water hyacinth plant leaves extract for colourimetric sensing of heavy metals, *Nano-Struct. Nano-Objects*, 2019, **20**, 100387.
- 21 D. Karthiga and S. P. Anthony, Selective colorimetric sensing of toxic metal cations by green synthesized silver nanoparticles over a wide pH range, *RSC Adv.*, 2013, **3**, 16765.
- 22 A. Bellingeri, M. Scattoni, I. Venditti, C. Battocchio, G. Protano and I. Corsi, Ecologically based methods for promoting safer nanosilver for environmental applications, *J. Hazard. Mater.*, 2022, **438**, 129523.
- 23 I. Corsi, I. Venditti, F. Trotta and C. Punta, Environmental safety of nanotechnologies: The eco-design of manufactured nanomaterials for environmental remediation, *Sci. Total Environ.*, 2023, **864**, 161181.



- 24 R. L. Hauke, A Taxonomic Monograph of Equisetum Subgenus Equisetum, *Nova Hedwigia*, 1979, **30**, 385–456.
- 25 T. Boeing, K. G. Tafarelo Moreno, A. Gasparotto Junior, L. Da Mota Silva and P. de Souza, Phytochemistry and Pharmacology of the Genus Equisetum (Equisetaceae): A Narrative Review of the Species with Therapeutic Potential for Kidney Diseases, *J. Evidence-Based Complementary Altern. Med.*, 2021, **2021**, 6658434.
- 26 S. Olsen, *Encyclopedia of garden ferns*, Timber Press, Portland, 2007.
- 27 M. Ihtisham, A. Noori, S. Yadav, M. Sarraf, P. Kumari, M. Brestic, M. Imran, F. Jiang, X. Yan and A. Rastogi, Silver Nanoparticle's Toxicological Effects and Phytoremediation, *Nanomaterials*, 2021, **11**, 2164.
- 28 S. Sedaghat and S. Omid, Batch process biosynthesis of silver nanoparticles using Equisetum arvense leaf extract, *Bioinspired, Biomimetic Nanobiomater.*, 2019, **8**, 190–197.
- 29 F. R. Cockerill, *Performance standards for antimicrobial susceptibility testing*, Twenty-third informational supplement; M100 - S23, CLSI, Wayne, PA, 2013.
- 30 P. Balashanmugam and P. T. Kalaichelvan, Biosynthesis characterization of silver nanoparticles using Cassia roxburghii DC. aqueous extract, and coated on cotton cloth for effective antibacterial activity, *Int. J. Nanomed.*, 2015, **10**, 87–97.
- 31 T. Kokila, P. S. Ramesh and D. Geetha, Biosynthesis of silver nanoparticles from Cavendish banana peel extract and its antibacterial and free radical scavenging assay: a novel biological approach, *Appl. Nanosci.*, 2015, **5**, 911–920.
- 32 S. Ghaffar, A. Abbas, M. Naeem-Ul-Hassan, N. Assad, M. Sher, S. Ullah, H. A. Alhazmi, A. Najmi, K. Zoghebi, M. Al Bratty, A. Hanbashi, H. A. Makeen and H. M. A. Amin, Improved Photocatalytic and Antioxidant Activity of Olive Fruit Extract-Mediated ZnO Nanoparticles, *Antioxidants*, 2023, **12**, 1201.
- 33 S. Sarkar, D. Modak, M. S. Haydar, J. J. George and S. Bhattacharjee, *Exploring the ameliorative role of Equisetum diffusum D. Don whole-plant methanolic-extract in acute inflammation and molecular docking analysis of GC-MS-identified phytochemicals with few prominent inflammatory markers/cytokines for inspecting the potent drug targets*, Research Square, Preprint 2023, DOI: [10.21203/rs.3.rs-2663599/v2](https://doi.org/10.21203/rs.3.rs-2663599/v2).
- 34 N. Mimica-Dukic, N. Simin, J. Cvejic, E. Jovin, D. Orcic and B. Bozin, Phenolic compounds in field horsetail (Equisetum arvense L.) as natural antioxidants, *Molecules*, 2008, **13**, 1455–1464.
- 35 S. Gurunathan, J.-K. Jeong, J. W. Han, X.-F. Zhang, J. H. Park and J.-H. Kim, Multidimensional effects of biologically synthesized silver nanoparticles in Helicobacter pylori, Helicobacter felis, and human lung (L132) and lung carcinoma A549 cells, *Nanoscale Res. Lett.*, 2015, **10**, 35.
- 36 J. Tiggesbäumker, L. Köller, K. H. Meiwes-Broer and A. Liebsch, Blue shift of the Mie plasma frequency in Ag clusters and particles, *Phys. Rev.*, 1993, **48**, R1749–R1752.
- 37 M. L. Firdaus, I. Fitriani, S. Wyantuti, Y. W. Hartati, R. Khaydarov, J. A. McAlister, H. Obata and T. Gamo, Colorimetric Detection of Mercury(II) Ion in Aqueous Solution Using Silver Nanoparticles, *Anal. Sci.*, 2017, **33**, 831–837.
- 38 K. Farhadi, M. Forough, R. Molaei, S. Hajizadeh and A. Rafipour, Highly selective Hg<sup>2+</sup> colorimetric sensor using green synthesized and unmodified silver nanoparticles, *Sens. Actuators, B*, 2012, **161**, 880–885.
- 39 S. Bothra, J. N. Solanki and S. K. Sahoo, Functionalized silver nanoparticles as chemosensor for pH, Hg<sup>2+</sup> and Fe<sup>3+</sup> in aqueous medium, *Sens. Actuators, B*, 2013, **188**, 937–943.
- 40 M. Sebastian, A. Aravind and B. Mathew, Green silver-nanoparticle-based dual sensor for toxic Hg(II) ions, *Nanotechnology*, 2018, **29**, 355502.
- 41 S. Balasurya, A. Syed, A. M. Thomas, N. Marraiki, A. M. Elgorban, L. L. Raju, A. Das and S. S. Khan, Rapid colorimetric detection of mercury using silver nanoparticles in the presence of methionine, *Spectrochim. Acta, Part A*, 2020, **228**, 117712.
- 42 I. Schiesaro, L. Burratti, C. Meneghini, I. Fratoddi, P. Proposito, J. Lim, C. Scheu, I. Venditti, G. Iucci and C. Battocchio, Hydrophilic Silver Nanoparticles for Hg(II) Detection in Water: Direct Evidence for Mercury–Silver Interaction, *J. Phys. Chem. C*, 2020, **124**, 25975–25983.
- 43 P. W. Atkins and J. de Paula, *Atkins' Physical chemistry*, W. H. Freeman, New York, 8th edn, 2006.
- 44 U. T. Khatoon, G. Nageswara Rao, K. M. Mohan, A. Ramanaviciene and A. Ramanavicius, Antibacterial and antifungal activity of silver nanospheres synthesized by tri-sodium citrate assisted chemical approach, *Vacuum*, 2017, **146**, 259–265.
- 45 J. K. Patra and K.-H. Baek, Antibacterial Activity and Synergistic Antibacterial Potential of Biosynthesized Silver Nanoparticles against Foodborne Pathogenic Bacteria along with its Anticandidal and Antioxidant Effects, *Front. Microbiol.*, 2017, **8**, 167.
- 46 N. Sanchooli, S. Saeidi, H. K. Barani and E. Sanchooli, In vitro antibacterial effects of silver nanoparticles synthesized using Verbena officinalis leaf extract on Yersinia ruckeri, Vibrio cholera and Listeria monocytogenes, *Iran. J. Microbiol.*, 2018, **10**, 400–408.
- 47 H. H. Lara, N. V. Ayala-Núñez, L. C. Del Ixtapan Turrent and C. Rodríguez Padilla, Bactericidal effect of silver nanoparticles against multidrug-resistant bacteria, *World J. Microbiol. Biotechnol.*, 2010, **26**, 615–621.
- 48 S. A. Ahmad, S. S. Das, A. Khatoon, M. T. Ansari, M. Afzal, M. S. Hasnain and A. K. Nayak, Bactericidal activity of silver nanoparticles: a mechanistic review, *Mater. Sci. Energy Technol.*, 2020, **3**, 756–769.

